

Multispectral Image Intrinsic Decomposition via Low Rank Constraint

Qian Huang
Nanjing University
cianhwang@gmail.com

Weixin Zhu
Nanjing University
njuzhwx@163.com

Yang Zhao
Nanjing University
zhaoyang@smail.nju.edu.cn

Linsen Chen
Nanjing University
njucls@163.com

Yao Wang
New York University
yw523@nyu.edu

Tao Yue
Nanjing University
yuetao@nju.edu.cn

Xun Cao
Nanjing University
caoxun@nju.edu.cn

Abstract

Multispectral images contain many clues of surface characteristics of the objects, thus can be widely used in many computer vision tasks, e.g., recolorization and segmentation. However, due to the complex illumination and the geometry structure of natural scenes, the spectra curves of a same surface can look very different. In this paper, a Low Rank Multispectral Image Intrinsic Decomposition model (LRIID) is presented to decompose the shading and reflectance from a single multispectral image. We extend the Retinex model, which is proposed for RGB image intrinsic decomposition, for multispectral domain. Based on this, a low rank constraint is proposed to reduce the ill-posedness of the problem and make the algorithm solvable. A dataset of 12 images is given with the ground truth of shadings and reflectance, so that the objective evaluations can be conducted. The experiments demonstrate the effectiveness of proposed method.

1. Introduction

The observed spectrum of a single pixel is determined by illumination, reflectance and shading. Shading image contains illumination condition and geometry information, while reflectance image contains the color information and material reflectance property, which are invariable to light condition and shadow effect. The decomposition problem has been a long standing problem of assorted areas such as both computer graphics and computer vision applications. For instance, shape-from-shading algorithms could benefit from an image with only shading effects, while image segmentation would be easier in a world without cast shadows.

Obviously, intrinsic image decomposition is an ill-posed problem, since there are more unknowns than observations. In order to solve this problem, many work [29, 30, 12] focus on sparse representation spatially, but this does not hold

for images in general. This paper addressed the problem of the recovery of reflectance and shading from a single multispectral image, namely, the Intrinsic Image Decomposition problem of a whole multispectral image captured under general spectral illumination, hereafter referred to as the IID problem. This problem is worth exploring since geometry and color information are useful under certain circumstances, but one of them always interferes the detection of the other one. Unfortunately, growing dimension of data makes this problem harder to cope with.

The low rank constraint that we proposed is based on the low rank prior, or low rank nature of both shading and reflectance images. According to the inherent nature of the multispectral image, we derive shading basis on the knowledge of illumination condition and derive reflectance subspace bases by means of principle component analysis (PCA) of Munsell color board. Assuming that the basis of Retinex theory would continue to take effect on multispectral domain, we proposed an low-rank-based model so that deriving reflectance and shading from a multispectral image can be modelled as an convex optimization problem. In a significant departure from the conventional approaches which operate in the logarithmic domain, we directly operate on the image domain to avoid adding additional noise or breaking low rank nature. The flowchart of our proposed algorithm for LRIID is shown in Fig. 1.

Suffering from the lack of ground truth data of shading and reflectance, we provide a ground-truth dataset for multispectral intrinsic images, which provides us a possible way to judge the quality of the decomposition results. Quantitative and qualitative experiments on our dataset have demonstrated that the performance of our work are better than prior work in multispectral domain. Our work can bring merits to multiple applications, such as recolorization, re-lighting, scene reconstruction and image segmentation.

Our major contribution can be summarized as follows: (1) we extend the Retinex model to multispectral image in-

trinsic decomposition problem, and propose a low rank constraint to handle the ill-posedness of the problem; (2) we provide a ground-truth dataset for multispectral intrinsic images, which can facilitate future evaluation and comparison of multispectral image intrinsic decomposition algorithms; (3) the proposed method achieves promising results on various of images both quantitatively and qualitatively.

2. Related Work

Intrinsic Image Decomposition. The problem of Intrinsic Image Decomposition (IID) was first introduced by Barrow and Tenenbaum [4]. The reflectance describes the illumination-invariant albedo of the surface, while the shading contains surface geometric information and illumination condition.

Assorted methods take advantage of additional information, including images sequences [33, 22] and videos [24] to avoid shadow effect in poor lighting condition. With the improvement of sensing devices like kinect, depth cue [2, 11, 24] or surface normal [27] have been applied to strengthen their assumption. More recently, Bousseau *et al.* [8] proposed a user-assisted method to further improve the result of separation.

Lots of methods with single input image are also proposed for the separation task. Bell *et al.* [6] developed a dense conditional random field (CRF) based intrinsic image algorithm for images in the wild. Barron *et al.* [3] introduced shape, illumination and reflectance from shading (SIRFS) model which performs well on images of segmented objects. Sai *et al.* [7] proposed L1 Image Transform model for scene-level intrinsic decomposition. Entropy method [13] raised by Finlayson *et al.* offered us a new viewpoint to understand this problem. With the abundance and availability of datasets and the development of computational equipment, training-based models [5, 32, 31, 37] have been built to derive reflectance and shading from images.

An especially well-know and wide-employed model called Retinex [23] made an assumption that the large chromatically change is generally caused by changes in reflectance rather than shading. With Retinex theory, we are able to pinpoint where the reflectance changes in local area. Horn, and Funt and Drew [16] analyzed local derivatives for distinguishing between image variations that are due to shading or reflectance. But it neglects the connection between pixels sharing the same neighborhood. On the basis of Retinex thoery, we follow work of Chen *et al.* [12] to handle intrinsic image decomposition task in multispectral domain.

Sparse Representation. Researchers have also extended trichromatic color constancy model to multispectral images

in order to separate reflectance and shading in higher spectral dimensions. A lot of trials have been made to explore this area. For example, Ikari *et al.* [18] showed us the possibility of separating dozens of multispectral signals. Huynh *et al.* [17] assumed that the scene could be segmented into several homogeneous surface patches, and were able to estimate the illumination and reflectance spectra under the dichromatic reflectance model. In remote sensing area, Kang *et al.* [20] fit multispectral data into trichromatic model to extract features.

To overcome the drawbacks of ambiguity in local analysis, lots of research have been done to reduce the ambiguity of both reflectance and shading. Shen *et al.* [29] proposed a global optimization algorithm which combines Retinex theory and non-texture constraint to obtain global consistency of image structures. Shen [30] further applied sparse representation of reflectance as global constraint of their observation. Material cues [26] has also been introduced. As to multispectral images, Chen *et al.* [12] used super-pixel to cut down the number of unknown parameters in this underdetermined problem. Unlike the approaches above, we assumed that both shading and reflectance live in low dimensional subspace. the low rank nature of shading space is widely acknowledged and exploited in prior work [16], and the low-dimensional subspace model of reflectance is introduced by [25, 28, 36]. With the help of training data of reflectance bases and illumination spectra, we can solve this problem effectively.

Dataset. As far as establishing ground-truth for intrinsic images, Tappen *et al.* [32] created small sets of both computer-generated and real intrinsic images. The computer-generated images consisted of shaded ellipsoids with piecewise-constant reflectance. The real images were created using green marker on crumpled paper [31]. Grosse *et al.* [15] provided an all-rounded dataset which is widely used in following analysis. Bell *et al.* [6] also introduced Intrinsic Images in the Wild, a large scale, public dataset for evaluating intrinsic image decompositions of indoor scenes. In multispectral field, [34, 10] provided a set of multispectral images of various objects without ground truth, and Chen *et al.* [12] built a dataset but the number, spectral resolution and diversity of images are limited. There is no other attempts to establish ground truth for multispectral intrinsic images.

3. Our Model

We assume the object surface as Lambertian and hence has diffuse reflection. In most prior work on intrinsic image decomposition, the captured luminance spectrum at every point l_p is modelled as the product of Lambertian reflectance spectrum r_p and shading spectrum s_p , where s_p

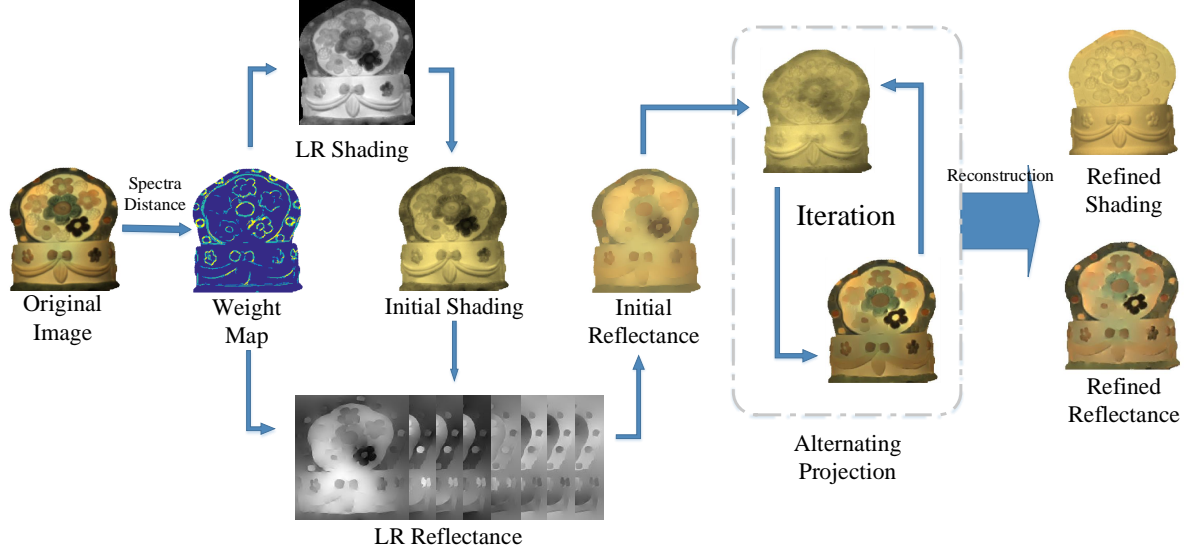


Figure 1. The flowchart of our proposed LRID algorithm.

is used to characterize the combined effect of object geometry, illumination, occlusion and shadowing. Mathematically, this model can be expressed as

$$l_p = s_p \cdot r_p \quad (1)$$

where l_p , r_p and s_p are all vectors with dimensions equal to the number of spectral bands of the captured image, \cdot denotes element-wise multiplication. The problem is to derive s_p and r_p from observed multispectral luminance vector l_p : In this project, we will focus on recovering the reflectance spectrum using this model. Once r_p is determined, the shading image can be derived by point-wise division.

Different from the conventional approaches which operate in the logarithmic domain, we directly formulate the problem in the image domain, and this can overcome numerical problems caused by the logarithmic transformation of the image values, where noise in pixels with low intensity values can lead to large variations. Besides, although there have been substantial evidence of the low rank nature of the reflectance space, it is not clear whether the logarithmically transformed reflectance space is still low rank. This makes it hard to incorporate the low rank prior in formulations based on log-transformed images.

3.1. Estimate Reflectance or Shading Independently

The Retinex model makes following two important observations:

- 1) When there is significant reflectance change between two adjacent pixels p and q , the shading is typically constant. This leads to the relation $l_p \cdot / l_q = r_p \cdot / r_q$, where $\cdot /$ denotes element-wise division;

- 2) When the expected reflectance difference between two pixels is small, the recovered reflectance difference between the two pixels should be small.

First we look at whether we can separate reflectance and shading from the measured luminance signal independently. Take reflectance for example. By recognizing two adjacent pixels which have the same shading, the ratio relationship can be written as $l_p \cdot r_q = l_q \cdot r_p$, or $L_p r_q = L_q r_p$ where L_p is a diagonal matrix consisting of spectral elements in l_p , we formulate the energy functions in terms of the reflectance vectors directly:

$$Esc = \sum_{p,q \in \mathcal{N}_{sc}} \|w_{p,q}(L_p r_q - L_q r_p)\|^d \quad (2)$$

$$Erc = \|v_{p,q}(r_p - r_q)\|^d$$

where \mathcal{N}_{sc} and \mathcal{N}_{rc} denote neighborhood pair sets and $w_{p,q}$ and $v_{p,q}$ denote weights. $w_{p,q}$ would be large but $v_{p,q}$ will be small when the expected reflectance difference between two adjacent pixels p and q are large, and vice versa. To make the formulation general, we use d to indicate the error norm, with $d = 2$ for L2 norm, and $d = 1$ for L1 norm. L1 norm is more difficult to solve, but the solution can be more robust to outliers.

If we directly solve for r_p , the above energy function can be written as the sum of K terms, one for each spectral component and each term can be separately minimized. With a little exercise, it can be shown that the minimal is achieved exactly when $r_p = l_p$; This is due to the inherent ambiguity of the problem, when no other constraints are imposed on r_p . we reduce the ambiguity by exploiting the fact that the reflectance spectra of typical object surfaces live in a low

dimensional subspace of R^K , so that any reflectance vector can be written as a linear combination of J_r basis, with $J_r < K$.

Let B_r represent the $K \times J$ basis matrix for representing the reflectance vector, r_p can be written as $r_p = B_r * \tilde{r}_p$. The energy function in Eq.(2) now becomes:

$$\begin{aligned} E_{sc} &= \sum_{p,q \in \mathcal{N}_{sc}} \|w_{p,q}(L_p B_r \tilde{r}_q - L_q B_r \tilde{r}_p)\|^d \\ E_{rc} &= \|v_{p,q}(B_r \tilde{r}_p - B_r \tilde{r}_q)\|^d \end{aligned} \quad (3)$$

The combined energy can be represented in a matrix form as:

$$E = \|W_{L,B_r} \tilde{R}\|^d + \lambda_1 \|V_{B_r} \tilde{R}\|^d \quad (4)$$

where \tilde{R} consists of \tilde{r}_p for all pixels in a vector. The matrix W_{L,B_r} depends on the neighborhood \mathcal{N}_{sc} considered, the weight $w_{p,q}$, the reflectance basis B_r used, and importantly the luminance data l_p ; whereas the matrix V_{B_r} depends on the neighborhood \mathcal{N}_{rc} considered, the weight $v_{p,q}$ and the reflectance basis B_r used. Therefore, with this non-logarithmic formulation, we encode the constraint due to the measured luminance data in the matrix W_{L,B_r} .

The ambiguity with the scaling factor is inherent in all intrinsic image decomposition problems since only the product of reflectance and shading is known. To circumvent the ambiguity about the scaling factor, we also explored another solution, where we express the generic constraint on the coefficient sum as $M\tilde{R} = C$, and augment the original energy function to enforce this constraint:

$$E_{\text{reft}} = \|W_{L,B_r} \tilde{R}\|^d + \lambda_1 \|V_{B_r} \tilde{R}\|^d + \lambda_2 \|M_r \tilde{R} - C\|^d \quad (5)$$

Similarly, the low rank nature of the shading space is also widely acknowledged and exploited in prior work [14]. Shading is inherently low rank, because there are usually only a few lighting sources with different illumination spectra acting in each captured scene, and the shading effect due to geometry and shadowing only modifies the spectra by a location-dependent scalar. If there is a single illumination source and its spectrum is known or is able to be identified by method of [36], we will use this spectrum(after normalization) as the only shading basis vector($J_s = 1$ and B_s equals to this normalized spectrum). Likewise the problem can be formulate as minimize

$$E_{\text{shad}} = \|W_{B_s} \tilde{S}\|^d + \lambda_1 \|V_{L,B_s} \tilde{S}\|^d + \lambda_2 \|M_s \tilde{S} - C\|^d \quad (6)$$

3.2. Simultaneous Recovery of Reflectance and Shading

Based on the formulation that solves reflectance and shading respectively, we proposed an optimization algorithm that simultaneously solves both shading and reflectance. We assume that the low rank subspace of the

shading and reflectance are known, represented by basis matrices B_s and B_r , respectively, so that $s_p = B_s \tilde{s}_p$ and $r_p = B_r \tilde{r}_p$. We will use \tilde{S} to denote the long vector consisting of shading coefficient vectors \tilde{s}_p at all pixels, and \tilde{R} the long vector consisting of reflectance coefficient vectors \tilde{r}_p . We propose to solve \tilde{s}_p and \tilde{r}_p , or equivalently \tilde{S} and \tilde{R} , by minimizing a weighted average of the following energy terms.

When shading is expected to be similar in pixels p and q , we have $s_p \approx s_q$ and $l_p * r_q \approx l_q * r_p$, or $L_p r_q = L_q r_p$, where L_p is a diagonal matrix consisting of spectral elements in l_p . We formulate the energy functions directly:

$$\begin{aligned} E_{sc} &= \sum_{p,q \in \mathcal{N}_{sc}} \|w_{p,q}(L_p r_q - L_q r_p)\|^d + \|w_{p,q}(s_p - s_q)\|^d \\ &= \|W_{L,B_r} \tilde{R}\|^d + \|W_{B_s} \tilde{S}\|^d \end{aligned} \quad (7)$$

When reflectance is expected to be similar in pixels p and q , we have $r_p \approx r_q$ and $l_p * s_q \approx l_q * s_p$, leading to a regularization energy

$$\begin{aligned} E_{rc} &= \sum_{p,q \in \mathcal{N}_{rc}} \|v_{p,q}(L_p s_q - L_q s_p)\|^d + \|v_{p,q}(r_p - r_q)\|^d \\ &= \|V_{L,B_s} \tilde{S}\|^d + \|V_{B_r} \tilde{R}\|^d \end{aligned} \quad (8)$$

The inherent data constraint $l_p = s_p * r_p$ leads to another energy function:

$$\begin{aligned} E_{\text{data}} &= \sum_p \|s_p * r_p - l_p\|^d = \|Q_{\tilde{S},B_s,B_r} \tilde{R} - L\|^d \\ &= \|Q_{\tilde{R},B_r,B_s} \tilde{S} - L\|^d \end{aligned} \quad (9)$$

where $Q_{\tilde{S},B_s,B_r}$ is a block diagonal matrix that depends on the solution for \tilde{R} and the basis matrices B_s and B_r (likewise $Q_{\tilde{R},B_r,B_s}$).

The problem is to find \tilde{S} and \tilde{R} that minimizes a weighted average of the three energy functions:

$$\begin{aligned} E &= E_{sc} + \lambda_1 E_{rc} + 2\lambda_{\text{data}} E_{\text{data}} \\ &= \|W_{L,B_r} \tilde{R}\|^d + \|W_{B_s} \tilde{S}\|^d + \lambda_1 (\|V_{L,B_s} \tilde{S}\|^d + \|V_{B_r} \tilde{R}\|^d) \\ &\quad + \lambda_{\text{data}} \|Q_{\tilde{S},B_s,B_r} \tilde{R} - L\|^d + \lambda_{\text{data}} \|Q_{\tilde{R},B_r,B_s} \tilde{S} - L\|^d \end{aligned} \quad (10)$$

Direct solution of the above problem solving s_p and r_p simultaneously is hard because of the bilinear nature of the data term. We applied iterative solution, where we solve \tilde{R} and \tilde{S} iteratively using alternating projection. As the dimension of the shading subspace is likely to be smaller than the dimension of the reflectance subspace, we solve the shading \tilde{S} first. Also there are typically more subregions in an image with similar reflectance, where it is easier to use the constant reflectance constraint to resolve the ambiguity about shading.

The only problem is that we need to give a initial estimation of \tilde{S} and \tilde{R} in order to effectuate the data constraint in Eq.(9). With the generic constraint in Part 3.1, Eq.(5) and Eq.(6), we give a previous estimation of \tilde{S} first, and then we can update \tilde{R} and find reflectance basis matrix, finally \tilde{R} and \tilde{S} are estimated respectively using the data constraint in Eq.(9).

More specifically, the whole recovery algorithm can be classified as Algorithm 1:

Algorithm 1: LRIID algorithm

- 1 **Step 1:** Assign constant-shading weights $w_{p,q}$ and constant-reflectance weights $v_{p,q}$.
 - 2 **Step 2:** Solve an initial low rank estimate of the shading image \tilde{S} using a generic constraint.
 - 3 **Step 3:** Solve an initial low rank reflectance estimate \tilde{R} using a generic constraint and the data constraint defined by the previous shading estimate.
 - 4 **repeat**
 - 5 **Step 4:** Solve \tilde{S} using the data constraint defined by the previous reflectance estimate.
 - 6 **Step 5:** Solve \tilde{R} using the data constraint defined by the previous shading estimate.
 - 7 **until** until the solution for \tilde{S} and \tilde{R} converge;
 - 8 **Step 6:** Reconstruct S and R to get the refined shading and reflectance.
-

4. Details

4.1. Weight Choice

As we know, images suffering from poor light condition may contain shadow area, which would in turn bring in unnecessary edges that confuse the algorithm. Various methods are used to determined weights $w_{p,q}$ and $v_{p,q}$, including pixel gradient [14, 21, 23], hue [35], correlation between vectors [19] and learning [32]. we proposed a illumination-robust and compute-friendly distance – normalized cosine distance, to signify the differences between spectra of pixels in one neighborhood. This distance can be formulated as

$$d_{p,q \in \mathcal{N}_{sc}} = 1 - \frac{l'_p l'_q}{|l'_p| \cdot |l'_q|} \quad (11)$$

$d_{p,q}$ tends to approximate to 0 when pixel p and q have same spectra, and depart from 0 when spectra of p and q are different. In order to derive weight $w_{p,q}$, we need to further magnify the difference between homogeneous and heterogeneous pixels and make it more robust to the noise. In our implementation

$$w_{p,q} = \frac{1}{1 + e^{\alpha(d_{p,q} - \beta)}} \quad v_{p,q} = 1 - w_{p,q} \quad (12)$$

α and β are parameters of sigmoid function. To set α and β , We sample 20 value of α within [1000, 10000] and 50 values of β within $[10^{-5}, 10^{-2}]$ and choose which perform best.

Fig. 2 shows different separation results when β changes. Local mean squared error (LMSE) is valued in 3 results. If β is too small, shading tends to be more blurred; while β is too big, reflectance would be blurred.

4.2. Low Rank Constraint

An important step to formulate a low rank constraint is to derive the low rank basis. With the help of multispectral imaging systems as PMIS [9] and CASSI [1], we can successfully get growth-truth illumination spectra. Also, there are plenty of work referring to how to extract illumination from the image. For example, [36] can be applied in multispectral domain and performs well in implementation. In order not to complicate our method, We simplify the process of getting normalized illumination spectra B_s by using the growth-truth illumination data.

When it comes to the low rank basis of reflectance, the authors of [25, 28] have found J_r to be around 8 so as to reach the best trade-off between expression power and noise resistance in the process of fitting reflectance spectra. we set J_r to be 8 and use the matrix introduced by [25] and perform Principle Component Analysis (PCA) to derive B_r from it.

4.3. Initial Estimation

In our implementation, only horizontally adjacent and vertically adjacent pixels are considered in the neighborhood N_{sc} and N_{rc} . Suppose there are N pixels in the image. The size of matrices W_{L,B_r} , V_{B_r} and \tilde{R} are $4NK \times NJ_r$, $4NK \times NJ_r$ and $NJ_r \times 1$ respectively in Eq.(3). Similarly, The size of matrices W_{B_s} , V_{L,B_s} and \tilde{S} in Eq.(6) are $4NK \times NJ_s$, $4NK \times NJ_s$ and $NJ_s \times 1$ respectively.

To avoid ambiguity, we further require that the shading image has small deviation from the input image. In Eq.(5), let M_r be a identity matrix, and C be a long vector concatenating all the pixels of the original image.

We use L2 form for all terms. so that the above problem for solving Eq.(5) or Eq.(6) is a quadratic programming problem, and can be solved efficiently using conjugated gradient method. In Algorithm 1, The solution to the unconstrained optimization problem in Step 2 satisfies the following linear equation

$$\lambda_2 M_s^T C = \left(W_{B_s}^T W_{B_s} + \lambda_1 V_{L,B_s}^T V_{L,B_s} + \lambda_2 M_s^T M_s \right) \tilde{S} = Q_s \tilde{S} \quad (13)$$

In Step 3, a data constraint defined by shading estimate need to be added to Eq.(5), so that the linear equation can

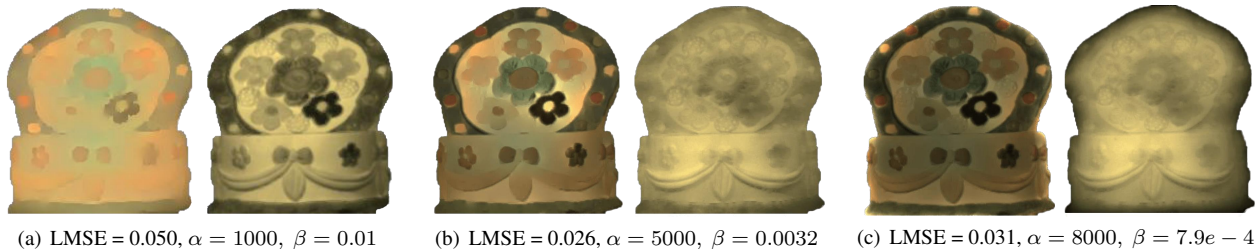


Figure 2. Results of threshold α and β . (b) achieves good result while shading and reflectance overlap clearly in (a) and (c).

be written as

$$\lambda_{\text{data}} Q_S^T L + \lambda_2 M_r^T C = \left(W_{L_r, B_r}^T W_{L_r, B_r} + \lambda_1 V_{B_r}^T V_{B_r} + \lambda_2 M_r^T M_r + \lambda_{\text{data}} Q_S^T Q_S \right) \tilde{R} = Q_r \tilde{R} \quad (14)$$

Because the matrix Q_r and Q_s is self-adjoint and sparse, we can solve this equation iteratively, which typically converges very fast. Here, λ_1 and λ_2 are positive weights for combining three different objective functions. In our implementation, we set $\lambda_1 = 2$, $\lambda_2 = 0.01$ and $\lambda_{\text{data}} = 1$ empirically.

4.4. Iteration Performance

We use alternating projection to get refined shading and reflectance. Just like what we stated in Step 4 and Step 5 in Algorithm 1, we update shading first and then the reflectance. In each round of iteration, gradient descent method is applied. Eq. 10 converges whenever it reaches the maximum iteration times 1000 or $\nabla E < 0.01$.

Fig. 3 demonstrates the iteration performance of our algorithm. Both cost function and LMSE decrease via iteration. Before the iteration, some shadow which should be the component of the shading image remains on the reflectance, while the brightness of the reflectance image tends to be uniform after iteration.

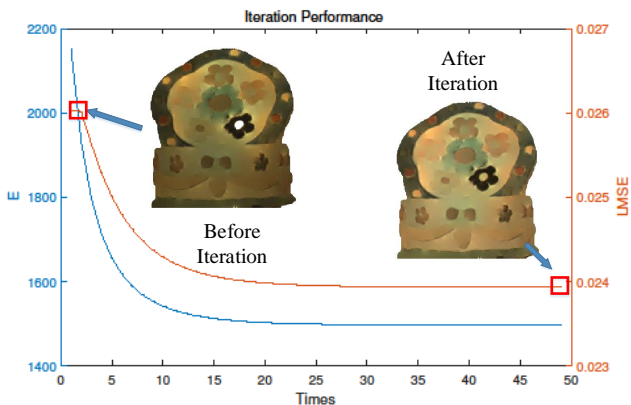


Figure 3. Iteration Performance. The algorithm converges within 50 times. Two images demonstrate the reflectance image which generated before and after iteration.

5. Experimental Results

In this section, we provide extensive experimental validation of the proposed method. For the better visualization, we show the result in pseudo-rgb and linearly normalized the image to the range $[0, 1]$. We first show the performance of our algorithm. This is followed by our method on on-line dataset and visual results. Finally, we test on our dataset with ground truth and compare our method with [12].

5.1. Experiments on proposed dataset

We provide a benchmark dataset with ground truth for the performance evaluation of multispectral image intrinsic decomposition problem. Following [15], we use local mean squared error (LMSE) from the ground truth to measure shading and reflectance image. We also compare with [12], which proposed intrinsic image decomposition algorithm in multispectral domain.

A benchmark dataset with ground-truth illumination, shading, reflectance and specularly was presented in [12] for performance evaluation of multispectral image intrinsic decomposition. Inspired by their ideas, we build up the newest multispectral intrinsic ground-truth dataset including 12 scenes under the same environmental conditions. We apply the updated mobile multispectral imaging camera to acquire the multispectral scenes, which could provide higher resolutions in spectral data ranging from 450nm-700nm with 118 spectral channels. Compared with the dataset provided by [12], ours is a similar but flowering in the diversity of projects with more detailed and bumpy scenarios which enables the dataset show further and potential applications in other vision researches (e.g. IRSS, segmentation and recognition).

Here, we evaluate our algorithm via our proposed dataset and use LMSE from the ground truth to validate our algorithm quantitatively. Compared with ground-truth, decomposition results that we achieved are desirable in terms of both the LMSE score (0.018 in average for the entire data set and the visual quality of the decomposed reflectance and shading results).

We display 4 examples from our dataset. For all the input diffuse images equipped with multispectral data with-

out the effect from illumination, the corresponding visualized RGB images for reflectance and shading are listed in Fig. 4 together with the LMSE results. It is clear that our method could produce pleasing visually decompositions based on multispectral images. In [12] generic constraint forces the sum value of a group of pixels to be a certain constant C, while in our method we let each pixel in shading image approximates to the pixel value of original image in the same position. Our generic constraint matrix is more sparse than that in [12], so that our algorithm will converge more quickly. What we have to emphasize here is that, we did all the image processing and metric computations of LMSE on down-sampled 30 out of 118 spectral channels (because [12] failed to process more bands on our 32G bytes memory) but all multispectral images are finally visualized above using corresponding synthesized RGB data.

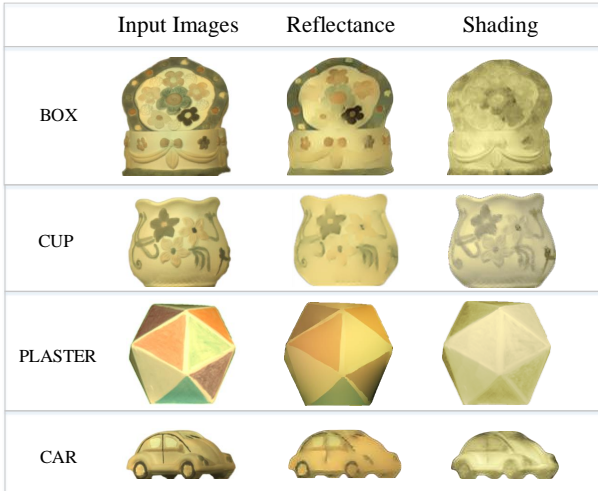


Figure 4. Results on sample images from the benchmark data set. we only show reflectance and shading color images synthesized from spectral data of 4 examples.

We display the computation time for examples in Fig. 4. Here SIID denotes spectral intrinsic image decomposition from the latest method based on Retinex in [12]. LRIID denotes the low rank multispectral image intrinsic decomposition from our algorithm. We compare the computation results obtained with and without low rank constraint. It can be seen that the low rank constraint helps to improve the computation time and decomposition results at the same time.

In table 1, we demonstrate the performance statics for dataset images. The last row shows the average metrics for the ground truth dataset. On average, the SIID method requires almost 11 seconds to process a multispectral image and generates results with 0.024 LMSE. While our method LRIID takes 1.739 seconds and produce results with 0.018 LMSE. Although we reduce the average LMSE slightly from 0.024 to 0.018, but the computation time is qualita-

Table 1. Performance statistics for dataset image

	Time(s)		LMSE	
	SIID	LRIID	SIID	LRIID
box	9.221	1.351	0.032	0.023
cup	7.610	0.675	0.016	0.012
car1	14.771	0.876	0.025	0.012
bottle1	11.275	0.666	0.062	0.031
bottle2	8.342	2.709	0.005	0.008
bottle3	7.993	2.337	0.009	0.009
bus	13.667	2.669	0.030	0.031
car2	7.643	1.807	0.030	0.024
dinosaur	13.465	2.306	0.021	0.023
minion	17.794	2.517	0.020	0.018
plane	10.763	2.125	0.024	0.015
train	9.108	0.832	0.017	0.015
Avg.	10.971	1.739	0.024	0.018

tively more efficient than that of SIID, and the running time approximates to the time in RGB cases in [29]. Moreover, We note that our method is memory-friendly and is able to process larger images with more spectral bands.

As to the reflectance, since it is not visualized from the spectral perspective, we try to compare the spectral curves of the reflectance from the ground truth and our algorithm. we choose patches in some scenes of our ground truth. In Fig. 5, it is obvious that our reflectance matches well with the ground truth which means we could gain accurate spectral reflectance with better performance in computation.

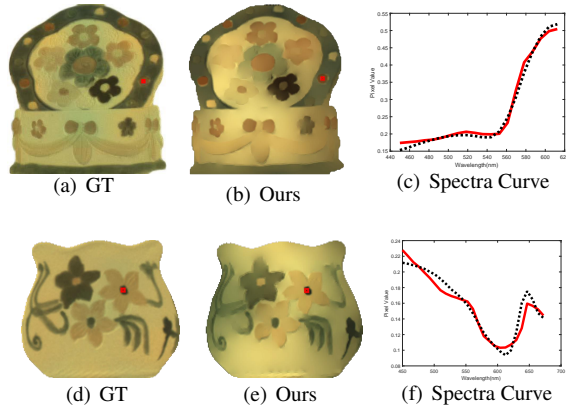


Figure 5. (a) and (d) are ground truth of our dataset, (b) and (e) are reflectance images of our results, and the (c) and (f) are spectra curve of marked area(solid red: curve of ours; dotted black: curve of ground-truth).

5.2. Experiments on Nayar multispectral image database[34]

A great variety of problems assume low-dimensional subspace structure and have been solved by adding low-

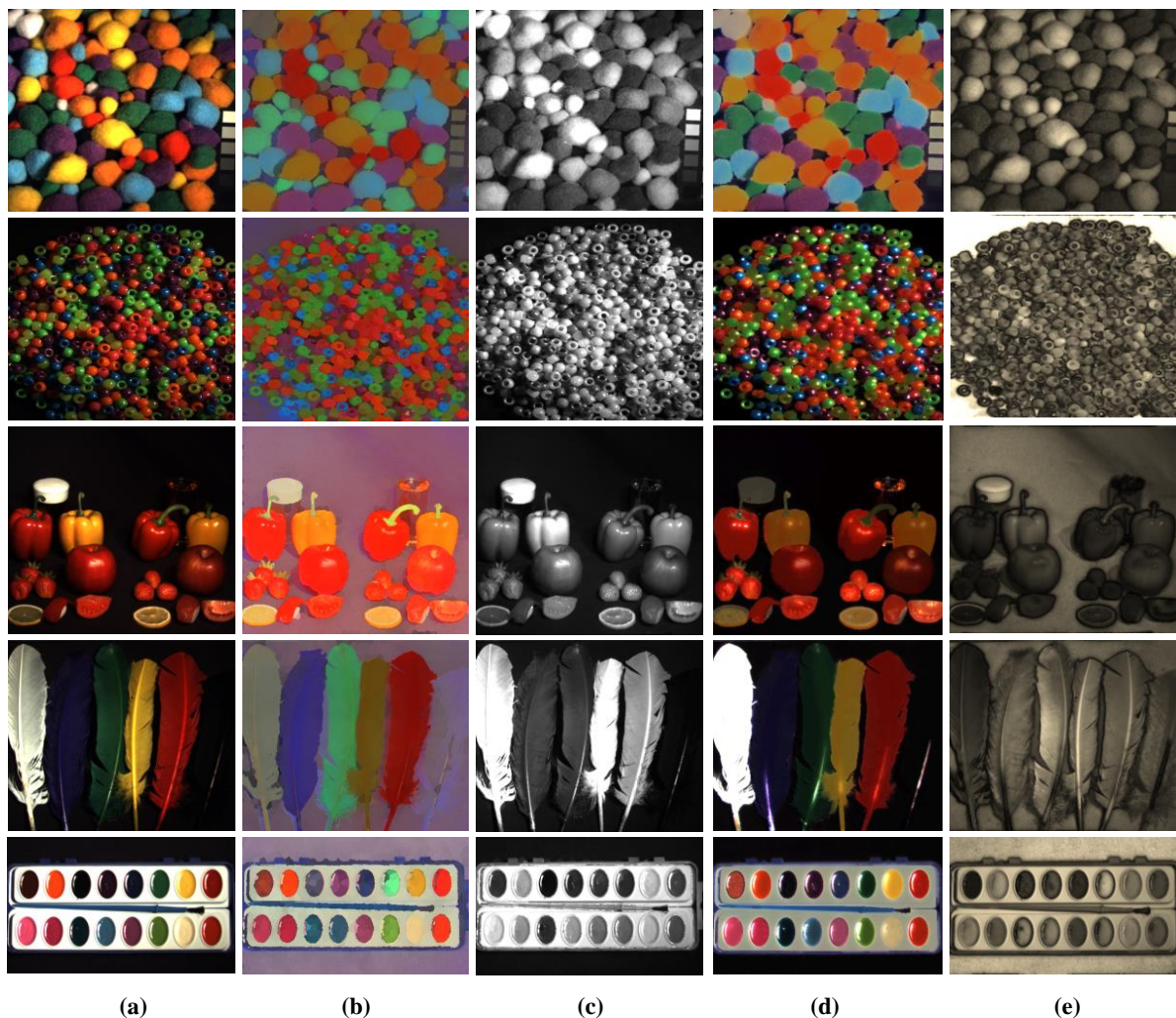


Figure 6. Comparison of decomposition without and with the low-rank constraint. (a) A single image for five different scenarios in Nayar dataset [34]. (b)-(c) and (d)-(e) show the reflectance and shading components computed by our LRIID solution without and with low-rank constraint, respectively. Note that both the original multispectral images (a) and multispectral reflectance (d) are integrated into 3-channel images by using the response curves of RGB sensors for visualization.

rank constraint, so is our method. To demonstrate the benefit of this constraint, we compare results with and without it in Fig. 6 using Nayar Multispectral Image Database [34]. The original images are shown in Fig. 6(a), the decomposed reflectance and shading without and with the low-rank constraint are shown in Fig. 6(b)-(e) respectively. From the comparison, we can see that the low-rank constraint helps to maintain global structures and improves decomposition results.

6. Conclusion

We have addressed the problem of the recovery of reflectance and shading from a single multispectral image captured under general spectral illumination. We have applied a low rank constraint to settle the multispectral image intrinsic decomposition problem, which significantly reduced the ambiguity. gradient descent has been used to give the initial estimation of reflectance and shading, and alternating projection method has been applied to solve the bilinear problem. Experiments on our dataset have demonstrated that the performance of our work are better than prior work in multispectral domain.

Our work has left out depth information. In fact, Retinex theory fails to take effect when both shading and reflectance change extensively in local area. Shading depends on the object surface geometry, which can be derived from depth information. We hope that we can make more accurate hypothesis about shading variation using the depth and surface normal information in the future.

References

- [1] G. R. Arce, D. J. Brady, L. Carin, H. Arguello, and D. S. Kittle. Compressive coded aperture spectral imaging: An introduction. *IEEE Signal Processing Magazine*, 31(1):105–115, 2014. [5](#)
- [2] J. T. Barron and J. Malik. Intrinsic scene properties from a single rgb-d image. In *Proceedings of the IEEE Conference on Computer Vision and Pattern Recognition*, pages 17–24, 2013. [2](#)
- [3] J. T. Barron and J. Malik. Shape, illumination, and reflectance from shading. *IEEE Transactions on Pattern Analysis and Machine Intelligence*, 37(8):1670–1687, 2015. [2](#)
- [4] H. Barrow and J. Tenenbaum. Computer vision systems. *Computer vision systems*, 2, 1978. [2](#)
- [5] M. Bell and E. Freeman. Learning local evidence for shading and reflectance. In *IEEE International Conference on Computer Vision*, volume 1, pages 670–677. IEEE, 2001. [2](#)
- [6] S. Bell, K. Bala, and N. Snavely. Intrinsic images in the wild. *ACM Transactions on Graphics*, 33(4):159, 2014. [2](#)
- [7] S. Bi, X. Han, and Y. Yu. An l1 image transform for edge-preserving smoothing and scene-level intrinsic decomposition. *ACM Transactions on Graphics*, 34(4):78, 2015. [2](#)
- [8] A. Bousseau, S. Paris, and F. Durand. User-assisted intrinsic images. In *ACM Transactions on Graphics*, volume 28, page 130. ACM, 2009. [2](#)
- [9] X. Cao, H. Du, X. Tong, Q. Dai, and S. Lin. A prism-mask system for multispectral video acquisition. *IEEE Transactions on Pattern Analysis and Machine Intelligence*, 33(12):2423–2435, 2011. [5](#)
- [10] A. Chakrabarti and T. Zickler. Statistics of Real-World Hyperspectral Images. In *Proceedings of the IEEE Conference on Computer Vision and Pattern Recognition*, pages 193–200, 2011. [2](#)
- [11] Q. Chen and V. Koltun. A simple model for intrinsic image decomposition with depth cues. In *Proceedings of the IEEE International Conference on Computer Vision*, pages 241–248, 2013. [2](#)
- [12] X. Chen, W. Zhu, Y. Zhao, Y. Yu, Y. Zhou, T. Yue, S. Du, and X. Cao. Intrinsic decomposition from a single spectral image. *Applied Optics*, 56(20):5676–5684, 2017. [1](#), [2](#), [6](#), [7](#)
- [13] G. D. Finlayson, M. S. Drew, and C. Lu. Intrinsic images by entropy minimization. In *European Conference on Computer Vision*, pages 582–595. Springer, 2004. [2](#)
- [14] B. V. Funt, M. S. Drew, and M. Brockington. Recovering shading from color images. In *European Conference on Computer Vision*, pages 124–132. Springer, 1992. [5](#)
- [15] R. Grosse, M. K. Johnson, E. H. Adelson, and W. T. Freeman. Ground truth dataset and baseline evaluations for intrinsic image algorithms. In *IEEE International Conference on Computer Vision*, pages 2335–2342. IEEE, 2009. [2](#), [6](#)
- [16] J. Ho, B. V. Funt, and M. S. Drew. Separating a color signal into illumination and surface reflectance components: Theory and applications. *IEEE Transactions on Pattern Analysis and Machine Intelligence*, 12(10):966–977, 1990. [2](#)
- [17] C. P. Huynh and A. Robles-Kelly. A solution of the dichromatic model for multispectral photometric invariance. *International Journal of Computer Vision*, 90(1):1–27, 2010. [2](#)
- [18] A. Ikari, R. Kawakami, R. T. Tan, and K. Ikeuchi. Separating illumination and surface spectral from multiple color signals. *Digitally Archiving Cultural Objects*, pages 297–321, 2008. [2](#)
- [19] X. Jiang, A. J. Schofield, and J. L. Wyatt. Correlation-based intrinsic image extraction from a single image. In *European Conference on Computer Vision*, pages 58–71. Springer, 2010. [5](#)
- [20] X. Kang, S. Li, L. Fang, and J. A. Benediktsson. Intrinsic image decomposition for feature extraction of hyperspectral images. *IEEE Transactions on Geoscience and Remote Sensing*, 53(4):2241–2253, 2015. [2](#)
- [21] R. Kimmel, M. Elad, D. Shaked, R. Keshet, and I. Sobel. A variational framework for retinex. *International Journal of Computer Vision*, 52(1):7–23, 2003. [5](#)
- [22] P.-Y. Laffont, A. Bousseau, and G. Drettakis. Rich intrinsic image decomposition of outdoor scenes from multiple views. *IEEE Transactions on Visualization and Computer Graphics*, 19(2):210–224, 2013. [2](#)
- [23] E. H. Land and J. J. McCann. Lightness and retinex theory. *Josa*, 61(1):1–11, 1971. [2](#), [5](#)
- [24] K. J. Lee, Q. Zhao, X. Tong, M. Gong, S. Izadi, S. U. Lee, P. Tan, and S. Lin. Estimation of intrinsic image sequences from image+ depth video. In *European Conference on Computer Vision*, pages 327–340. Springer, 2012. [2](#)
- [25] L. T. Maloney. Evaluation of linear models of surface spectral reflectance with small numbers of parameters. *JOSA A*, 3(10):1673–1683, 1986. [2](#), [5](#)
- [26] A. Nadian-Ghomsheh, Y. Hassanian, and K. Navi. Intrinsic image decomposition via structure-preserving image smoothing and material recognition. *PloS one*, 11(12):e0166772, 2016. [2](#)
- [27] R. A. Newcombe, S. Izadi, O. Hilliges, D. Molyneaux, D. Kim, A. J. Davison, P. Kohi, J. Shotton, S. Hodges, and A. Fitzgibbon. Kinectfusion: Real-time dense surface mapping and tracking. In *IEEE International Symposium on Mixed and Augmented Reality*, pages 127–136. IEEE, 2011. [2](#)
- [28] J. P. Parkkinen, J. Hallikainen, and T. Jaaskelainen. Characteristic spectra of munsell colors. *JOSA A*, 6(2):318–322, 1989. [2](#), [5](#)
- [29] L. Shen, P. Tan, and S. Lin. Intrinsic image decomposition with non-local texture cues. In *IEEE Conference on Computer Vision and Pattern Recognition*, pages 1–7. IEEE, 2008. [1](#), [2](#), [7](#)
- [30] L. Shen, C. Yeo, and B.-S. Hua. Intrinsic image decomposition using a sparse representation of reflectance. *IEEE Transactions on Pattern Analysis and Machine Intelligence*, 35(12):2904–2915, 2013. [1](#), [2](#)

- [31] M. F. Tappen, E. H. Adelson, and W. T. Freeman. Estimating intrinsic component images using non-linear regression. In *IEEE Computer Society Conference on Computer Vision and Pattern Recognition*, volume 2, pages 1992–1999. IEEE, 2006. [2](#)
- [32] M. F. Tappen, W. T. Freeman, and A. E. H. Recovering intrinsic images from a single image. In *IEEE Transactions on Pattern Analysis and Machine Intelligence*, volume 27, pages 1459–1472, 2005. [2](#), [5](#)
- [33] Y. Weiss. Deriving intrinsic images from image sequences. In *IEEE International Conference on Computer Vision*, volume 2, pages 68–75. IEEE, 2001. [2](#)
- [34] F. Yasuma, T. Mitsunaga, D. Iso, and S. K. Nayar. Generalized assorted pixel camera: postcapture control of resolution, dynamic range, and spectrum. *IEEE Transactions on Image Processing*, 19(9):2241–2253, 2010. [2](#), [7](#), [8](#)
- [35] Q. Zhao, P. Tan, Q. Dai, L. Shen, E. Wu, and S. Lin. A closed-form solution to retinex with nonlocal texture constraints. *IEEE Transactions on Pattern Analysis and Machine Intelligence*, 34(7):1437–1444, 2012. [5](#)
- [36] Y. Zheng, I. Sato, and Y. Sato. Illumination and reflectance spectra separation of a hyperspectral image meets low-rank matrix factorization. In *Proceedings of the IEEE Conference on Computer Vision and Pattern Recognition*, pages 1779–1787, 2015. [2](#), [4](#), [5](#)
- [37] T. Zhou, P. Krahenbuhl, and A. A. Efros. Learning data-driven reflectance priors for intrinsic image decomposition. In *Proceedings of the IEEE International Conference on Computer Vision*, pages 3469–3477, 2015. [2](#)